

RESEARCH

Open Access



Neurodegeneration and contralateral α -synuclein induction after intracerebral α -synuclein injections in the anterior olfactory nucleus of a Parkinson's disease A53T mouse model

Alicia Flores-Cuadrado¹, Daniel Saiz-Sanchez¹, Alicia Mohedano-Moriano², Alino Martinez-Marcos¹ and Isabel Ubeda-Bañon^{1*} 

Abstract

Parkinson's disease is characterized by a proteinopathy that includes aggregates of α -synuclein. A recent hypothesis proposes a prion-like spreading mechanism for this α -synucleinopathy. Early neuropathological deposits occur, among others, in the anterior olfactory nucleus (AON). This study investigates the anterograde and/or retrograde transmissibility of exogenous α -synuclein inoculated in the right AON of the A53T model of Parkinson's disease and wild-type mice as well as neuronal and glial involvement. Seven experimental groups were established: wild-type injected with tracers; A53T mice injected with either α -synuclein or saline 2 months beforehand; wild-type injected with either α -synuclein or saline 2 months beforehand; and wild-type injected with either α -synuclein or saline 4 months beforehand. Weight and behavioral changes were analyzed. Immunohistochemistry against α -synuclein, NeuN, Iba-1 and GFAP was performed. Volume and marker distributions in the olfactory bulb (OB), AON and piriform cortex were analyzed using unbiased stereology. The behavioral analyses reveal higher levels of hyperactivity in transgenic as compared to wild-type mice. Tract-tracing experiments show that the main contralateral afferent projections to the dorsal AON come from the AON and secondarily from the OB. In saline-injected transgenic animals, α -synuclein expression in the OB and the AON is higher in the left hemisphere than in the right hemisphere, which could be due to basal interhemispheric differences. α -synuclein injection could provoke a significant increase in the left hemisphere of the transgenic mice's OB, compared to saline-injected animals. Neuronal loss was observed in saline-injected transgenic mice relative to the saline-injected wild-type group. There were no overall differences in neuron number following injection of α -synuclein into either wild-type or transgenic mice, however some neuron loss was apparent in specific regions of α -synuclein injected wild-types. Microglia labeling appeared to be correlated with surgery-induced inflammation. Astroglial labeling was higher in transgenic animals, which could be due to endogenous α -synucleinopathy. This study suggests α -synucleinopathy induction, via retrograde and contralateral projections, within the olfactory system of transgenic animals.

Keywords: α -Synucleinopathy, Astroglia, Microglia, Neurodegeneration, Non-motor symptoms, Olfaction, Stereology

* Correspondence: Isabel.ubeda@uclm.es

¹Neuroplasticity and Neurodegeneration Laboratory, CRIB, Ciudad Real Medical School, University of Castilla-La Mancha, Camino de Moledores s/n, Ciudad Real 13071, Spain

Full list of author information is available at the end of the article



Introduction

Parkinson's disease (PD) is the second most prevalent neurodegenerative disease (affecting 2–3% of the population \geq 65 years of age). It is mostly idiopathic and clinically diagnosed with the presence of bradykinesia in combination with rigidity and/or rest tremor [56, 59]. Motor symptoms are due to neuronal loss of dopaminergic cells in the substantia nigra pars compacta and the corresponding striatal denervation [39]. A prodromal period characterized by non-motor features, such as rapid eye movement sleep behavior disorder, constipation and hyposmia has been described [17, 70, 71]. PD is a synucleinopathy characterized by aggregates of α -synuclein and ubiquitin (Lewy bodies and neurites) which follows a progressive and predictable staging pattern [5], although the correlation between clinical manifestations and pathological deposits is far from straightforward [36]. Interestingly, Lewy pathology first appears in the dorsal motor nucleus of the vagus nerve and in the olfactory bulb (OB) [14, 15], particularly in the anterior olfactory nucleus (AON) [2, 4, 12, 72, 76, 77, 79].

The idea that proteinopathies associated with neurodegenerative diseases could spread in a prion-like manner, thus helping to explain their etiology, was proposed more than three decades ago [38, 60–62, 83]. Prion-like hypothesis is based on a conformational change from α -helix native α -synuclein into β -sheet form through a seeding mechanism and subsequent spreading process [29]. Unfolded α -synuclein monomers are able to turn into oligomers, and thereafter to amyloid fibrils. These fibrils give rise to Lewy bodies formation within neurons and glial cells [28, 42]. In the last decade this hypothesis has been supported by experimental data in PD [8, 74]. In vitro and in vivo data regarding neuronal α -synuclein spreading have been obtained in several species, and a number of mechanisms have been proposed for axonal [13] and transneuronal transport [18, 33, 74]. Further, it has been demonstrated in vitro that astrocytes can take up α -synuclein through an endocytic event and spread this α -synuclein to neurons, hence leading to neural death [10], although, in vivo, glial role on this process has been hardly investigated.

Neuroinflammation is a complex and dynamic response involved in PD. It has been suggested that microglia and astroglia have a major role in the onset, progression [27, 34] and degeneration associated to PD [7, 43]. The crosstalk between α -synuclein and glial cells is particularly interesting since α -synuclein is able to activate and direct microglia and its migration [40]. Also, microglia is responsible of clearing extracellular α -synuclein [44]. This microgliosis has been observed in PD post-mortem areas [19], including OB [41], in vivo, using PET imaging in prodromal (REM sleep disorder patients) and diagnosed PD patients [23, 75] and also in mouse models [43].

Not only microglia is relevant in PD, α -synuclein aggregates have been also reported in astrocytes [6]. A53T α -synuclein exclusively expressed in astrocytes, it is able to accelerate onset of movement disorders, disease progression and inflammatory response in mice [30]. Astrocytes establish communications with neurons, microglia and other astrocytes. Among their main roles are: homeostasis, injury repair and inhibition of microglial activation in healthy brain [32, 37]. Astroglia become active in diseased brain to protect neurons from oxidative stress and prevent excessive inflammation. In fact, some PD related genes are expressed in astrocytes and microglia [37]. There are multiple mechanisms by α -synuclein spreading as an intercellular transfer. α -Synuclein fibrils could transfer from neuron to neuron and from neuron to glial cells, even these cells are able to internalize them [1]. In fact, it has been suggested that glial cells have a dual role as collaborators in the α -synuclein spreading or/and its degradation [47].

Hodologically, several studies have demonstrated neural transmission of exogenous, intracerebrally injected α -synuclein in connected areas involved in PD: striatal injections and retrograde transport to the substantia nigra pars compacta [48]; nigral injections and anterograde and retrograde transport in the hippocampus, amygdala, hypothalamus and cortex [52]; vagal injections and retrograde transport in the locus coeruleus, dorsal raphe nucleus, hypothalamus and amygdala [81]; OB injections and anterograde and retrograde transport in olfactory structures [64] and beyond, including the substantia nigra [63]; and OB/AON injections and retrograde and anterograde transport in olfactory and hippocampal structures [51].

The OB has been identified as a key structure for the prion-like spreading of α -synuclein, as hyposmia is an early manifestation of the disease and Lewy pathology occurs in the OB and AON during Braak's stage I [65]. The olfactory mucosa is exposed to the environment and directly connected to the OB, which in turn sends projections to the cortex without thalamic relay [31, 50]. Further, the olfactory system is characterized by massive centrifugal projections in which the AON is reciprocally and bilaterally connected [53]. The OB and AON are not only early and preferentially involved in α -synucleinopathy in humans [76, 77, 79], but also in transgenic mouse models [78, 80].

Despite a number of investigations have injected different kinds of α -synuclein in rodents, few of them include injections on OB/AON [51, 63, 64, 74]. In addition, A53T is a suitable model for α -synucleinopathy investigation in olfactory structures [20, 21, 78, 80]. As far as we know, the present report is the first to include injections restricted to the AON in both WT and TG mice.

The aim of this study was, therefore, to validate α -synucleinopathy induction (seeding and spreading) of

exogenously injected α -synuclein in the context of prion-like hypothesis in PD [82]. In this study the AON, OB and Pir have been analyzed bilaterally to evaluate possible anterograde and/or retrograde α -synucleinopathy induction including seeding and spreading mechanisms. This is particularly interesting using a model that endogenously overexpress α -synuclein [49] and comparing it with control mice. The concrete objectives of this study were to analyze behavioral changes, connectional spreading, neuronal and glial (microglia and astroglia) involvement after α -synuclein injections in the right AON of both a transgenic PD A53T model (TG) and wild-type mice (WT). To our knowledge this is the first study to include not only WT, but also TG mouse models overexpressing α -synuclein. This allows comparison on the role of endogenously overexpressed human pathological α -synuclein vs. exogenously injected human physiological α -synuclein on seeding and spreading mechanisms along known projections as well as neuronal and glial involvement.

Material and methods

Experimental animals

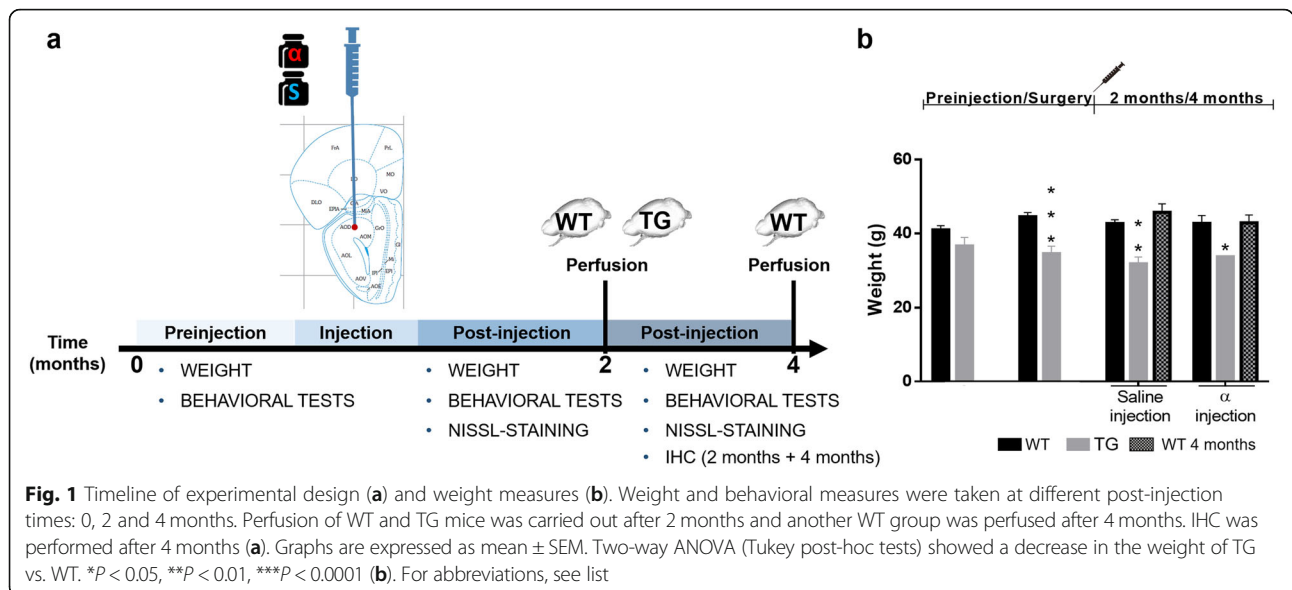
Forty-four adult male wild-type (WT, B6C3F1/J) and homozygous transgenic (TG, B6; C3-Tg-Prnp-SNCA^{A53T}-83V1e/J; 004479, The Jackson Laboratory, USA) mice were initially used for this study. One group of WT animals was used for tract-tracing experiments. Behavioral analyses were carried out on the remaining animals pre- and post-injection of α -synuclein or saline prior to sacrifice after either 2 or 4 months (Fig. 1a). The initial design of the study thus included nine experimental groups: $n = 4$ for tract-tracing experiments and $n = 5$ each for α -synuclein or saline injections, in TG

or WT animals, surviving either 2 or 4 months. At the time of the injection, the average age of animals was 46.63 ± 0.18 (SEM) weeks. Given the high degree of mortality among animals after the injection (especially among TG), TG groups to be sacrificed after 4 months were not included in the final analysis; instead, they were incorporated into the group to be sacrificed after 2 months. Mice were thus divided into seven groups at the end of the investigation. Group 1: WT tract-tracing dextran amine experiments ($n = 4$); groups 2 and 3: TG α -synuclein ($n = 3$) or saline ($n = 4$) surviving 2 months; groups 4 and 5: WT α -synuclein ($n = 4$) or saline ($n = 4$) surviving 2 months; and groups 6 and 7: WT α -synuclein ($n = 4$) or saline ($n = 5$) surviving 4 months; totaling 28 animals at the end of the study. The animals were housed in experimental groups on a standard 12 h/12 h light/dark cycle, at 21 °C, with food and water ad libitum. All experiments carried out were in agreement with European (Directive 2010/63/EU) and Spanish (RD 53/2013) regulations on the protection of animals used for scientific purposes, and they were also approved by the Ethical Committee for Animal Research of the University of Castilla-La Mancha (SAF2016–75768-R).

Behavioral analyses

Corner test

Following the protocol established by [3], a corner test was performed for 30 s. Briefly, animals were individually placed in the center of a clean standard home cage (30.5 cm \times 26.5 cm), filled with wood shavings. The number of corners visited, the latency to reach the first corner, the latency to the first rearing and the number of rearings were all recorded and measured.



Open-field test

Mice were placed in the center of an open field (a hand-made, white wooden box, 55 cm × 55 cm × 25 cm) and observed for 5 min. The following sequence of behavioral events was recorded: latency to leave the central square, latency to enter the peripheral zone, number of rearings and number of crossings. During the test, the numbers of defecation boli and urination episodes were also recorded (data not shown) [3].

Rotarod

The LE-8500 rotarod (PanLab/Harvard Apparatus, Barcelona, Spain) was used to examine motor impairment. Each mouse was placed with its head against the direction of rotation. The drum was slowly accelerated from a speed of 4–40 rpm over a 300-s period. The latency to fall from the rotarod within this period was recorded by SeDaCom 2.0 software (PanLab/Harvard Apparatus, Barcelona, Spain). Mice underwent five consecutive trials in one day. The mean latency to fall from the rotarod and the speed for independent and combined trials were analyzed [55, 58].

Wire hang test

In the wire hang test, a horizontal wire (diameter 2 mm, length 40 cm) divided into 4 segments was suspended at a height of 80 cm over a cage filled with bedding to avoid injury when falling. The animal was placed clinging to the middle of the wire with its forepaws during one 60-s trial. Motor coordination was measured as the number of segments crossed and muscle strength until falling from the wire [25].

Tracer injections

Four animals were anesthetized with a combined dose of ketamine hydrochloride (Ketolar, Parke-Davis, Madrid, Spain; 1.5 mL/kg, 75 mg/kg) and xylazine (Xilagesic, Calier, Barcelona, Spain; 0.5 mL/kg, 10 mg/kg). Eye drops (Lacryvisc, Alcon, Barcelona) were applied to prevent eye ulceration during surgery. Under stereotaxic control (anterior 2.8 mm; lateral 1 mm; depth –2.7 mm, from dura mater) [22], rhodamine-labeled dextran amine (RDA) and fluorescein-labeled dextran amine (FDA) (10,000 mW, lysine fixable, Molecular Probes, Eugene, OR; 10% diluted in PBS) were iontophoretically injected (30–80 μm tip diameter; positive current pulses 7/7 s; 2–7 μA; 8–20 min) at the right and left dorsal AON, respectively.

α-Synuclein and saline injections

For microinjections, mice were grouped as described above and injected with recombinant α-synuclein (Sigma Aldrich® S7820, human origin, physiological form, N-terminal histidine tagged 140-amino acid protein, 19–20 kDa apparent

molecular weight, encoded by a simple gene consisting of six exons on human chromosome 4, expressed in *E. coli*, supplied as lyophilized powder) or saline in the right AON. Animals were anesthetized as described above. Using the same stereotaxic coordinates as used for tracers, 2 μL of 2 μg/μL of α-synuclein in saline or only saline were injected in a constant infusion (0.2 μg per minute) for 10 min using a microsyringe (10 μL Neuros Model 1701 RN, point style 4; SYR, Hamilton Co., Reno, Nevada, USA). Animals were kept on the stereotaxic apparatus for 5 additional minutes to improve the diffusion of the extract before removing the syringe.

Perfusion and tissue section

Animals injected with tracer were perfused one week post-injection. Animals injected with α-synuclein or saline were perfused either 2 or 4 months after injection. Mice were anesthetized (as described above) and perfused with saline solution followed by 4% w/v para-formaldehyde fixative (phosphate buffered; 0.1 M sodium phosphate, pH 7.2). Brains were post-fixed in 4% w/v para-formaldehyde and cryoprotected in 30% w/v sucrose. Finally, brains were frontally sectioned using a freezing microtome, and 50-μm sections were sequentially collected in eight-section series.

Mounting and analyzing sections with fluorescent tracers

Sections were counterstained with 4'6-diamidino-2-phenylindole (DAPI) (Sigma-Aldrich Co. Ltd.) for 5 min in the dark, mounted and coverslipped with antifading polyvinyl alcohol mounting medium (Sigma-Aldrich Co. Ltd.). Images were taken using a confocal microscope LSM 800 (Zeiss, Jena, Germany). Contrast and brightness were adjusted using Image J software.

Immunohistochemical procedures

For α-synuclein and ionized calcium-binding adaptor molecule 1 (Iba-1) immunohistochemistry, endogenous peroxidase activity was inhibited by bathing twice for 15 min in 1% H₂O₂ in phosphate-buffered saline (PBS) (0.01 M pH 7.4). After washes, sections were incubated for 2 h in blocking buffer (0.3% TX-100, 5% normal horse serum with PBS 0.01, pH 7.4). Subsequently, sections were incubated at 4 °C overnight in blocking buffer with primary antibodies (Additional file 1: Table S1). For neuronal marker (NeuN) and glial fibrillary acidic protein (GFAP) immunohistochemistry, endogenous peroxidase activity was inhibited by a 20-min bath in 1% H₂O₂ in PBS. After washes, sections were incubated for 2 h in PBS with 0.1% TX-100 (Iba-1) or 0.3% TX-100 (NeuN). Then sections were incubated in PBS with 0.1% TX-100 (Iba-1) or 0.3% TX-100 (NeuN) with primary antibodies at 4 °C overnight (Additional file 1: Table S1).

After washes, sections were incubated for 2 h in secondary biotinylated antibodies in blocking buffer (Additional file 1: Table S1); for NeuN and GFAP, sections were incubated without normal horse serum. Sections for immunohistochemistry were incubated in avidin-biotin complex (ABC Standard, Vector Laboratories), reacted using 0.025% 3,3'-diaminobenzidine and 0.1% H₂O₂. Then sections were cresyl violet counterstained (Sigma Aldrich, C5042). The protocol was as follows: dip in distilled H₂O for 2 min; incubate slides in cresyl violet 0.1% for 1 min; take out the slides, removing the excess by tapping on the container; quickly dip the slides 8 times in 96% ethanol, and then 8 times in 100% ethanol; leave slides in xylene I for 1 min and xylene II for 2 min; cover-slip with DPX (Sigma Aldrich, 06522). Controls included omitting primary antibodies, secondary antibodies, and using tissue from WT animals.

Unbiased, design-based stereology

Quantification was carried out using Stereo Investigator software (MBF Bioscience; microscope Zeiss Axio Imager M2), which is composed of an optical fractionator stereology probe. Stereological techniques are unbiased three-dimensional counting methods using random frames over regions of interest. This probe estimates the number of human α -synuclein aggregates found in cell bodies (aggregates in neurites were not considered), NeuN or Iba-1-positive cells and sub-volumes in the optical dissector (virtual space) in a thick tissue section. Afterwards, these sub-volumes were extrapolated to estimate the entire cell population (cells/mm³). The methodology is based on detection of the top-edge of the cell in the dissector and having enough focal planes to determine whether it is in the dissector, using a 63 \times oil objective and z-axis. This rule is useful to prevent overestimation. Prior to counting aggregates or cells, data such as the number of sections, thickness (50 μ m) and interval between sections (eight) were added to the software [26].

OB, AON and piriform cortex (Pir) boundaries were traced using cresyl violet staining at 5 \times magnification. In addition, OB layers (glomerular, GL; external plexiform, EPL; mitral, MiL; internal plexiform, IPL and granule, GrL layers) were also drawn for Iba-1 staining. Tissue was then examined at high magnification (Plan Apochromat, 63 \times / 1.4, Oil lens, Ref: 420782–9900). The parameters of grid size and counting frame were adapted to α -synuclein, NeuN and Iba-1 markers and the size of different layers (Additional file 1: Table S2). Section thickness was measured at each counting site. Both α -synuclein aggregates, NeuN and Iba-1-positive cells were counted by placing a marker on each within the counting frame whilst not touching the red exclusion line.

Area fraction

Given the number of fibers in GFAP-positive cells, optical dissector analysis was ruled out. The images, taken with a Nikon Eclipse 80i, were captured from each section and hemisphere (OB $n = 2$, 6–9 sections per hemisphere; AON $n = 2$, 3–4 sections per hemisphere; Pir $n = 2$, 4–5 sections per hemisphere; 24 animals; $N = 1550$ pictures). Images were processed with ImageJ and converted to 8-bit gray scale. Afterwards, we analyzed the generated histogram. The histogram mode was multiplied by 0.7 to obtain the threshold and measure the area fraction.

Statistical analysis

Statistical analysis was performed using Graphpad Prism software (v6.01; La Jolla, CA). A Shapiro-Wilk test ($N < 50$) was carried out to analyze the normality. A statistical comparison was analyzed using two-way ANOVA (Tukey post-hoc test) or Kruskal-Wallis non-parametric test (Dunn's multiple comparisons test), with the following variables: treatment (saline or α -synuclein injection), genotype (WT or TG), time (only for WT, 2 or 4 months survival) or hemisphere (left, LH, or right, RH). Two-tailed and Mann-Whitney tests were only applied when the P -value of the source of variation (treatment, genotype, time or hemisphere effect) was significant. Differences were regarded as statistically significant at * or # $P < 0.05$; ** or ## $P < 0.01$; *** or ### $P < 0.001$; **** or #### $P < 0.0001$. Significant results are described in the text and/or figures. Statistical data are included in the Additional file 2: Figure S1–S4, Additional file 3: Tables S3–S7 and Additional file 4: Tables S8–S17.

Results

As described above, although initially nine experimental groups were established, at the end of the investigation only seven were used: one group for tract-tracing experiments and the remaining six groups for α -synuclein or saline injections with different survival times (Fig. 1a). Since behavioral analysis concluded that most effects were due to genotype, but not to experimental procedures, all these results were included in Additional file 2. Similarly, since volume analysis did not report a clear trend, most of these data were included in Additional file 3: Tables S3–S7 and Figure S5. Finally, the injection sites for saline or α -synuclein showed a different appearance depending on the marker used (α -synuclein, Iba-1 or GFAP) (Additional file 4: Figure S6).

Weight

Animals were weighed during the experimental procedure. Weight loss was observed in TG as compared to WT mice, even before injections (Interaction: $F(3, 64) = 1.120$, $P = 0.3478$; Treatment effect: $F(3, 64) = 0.5025$, $P = 0.6819$;

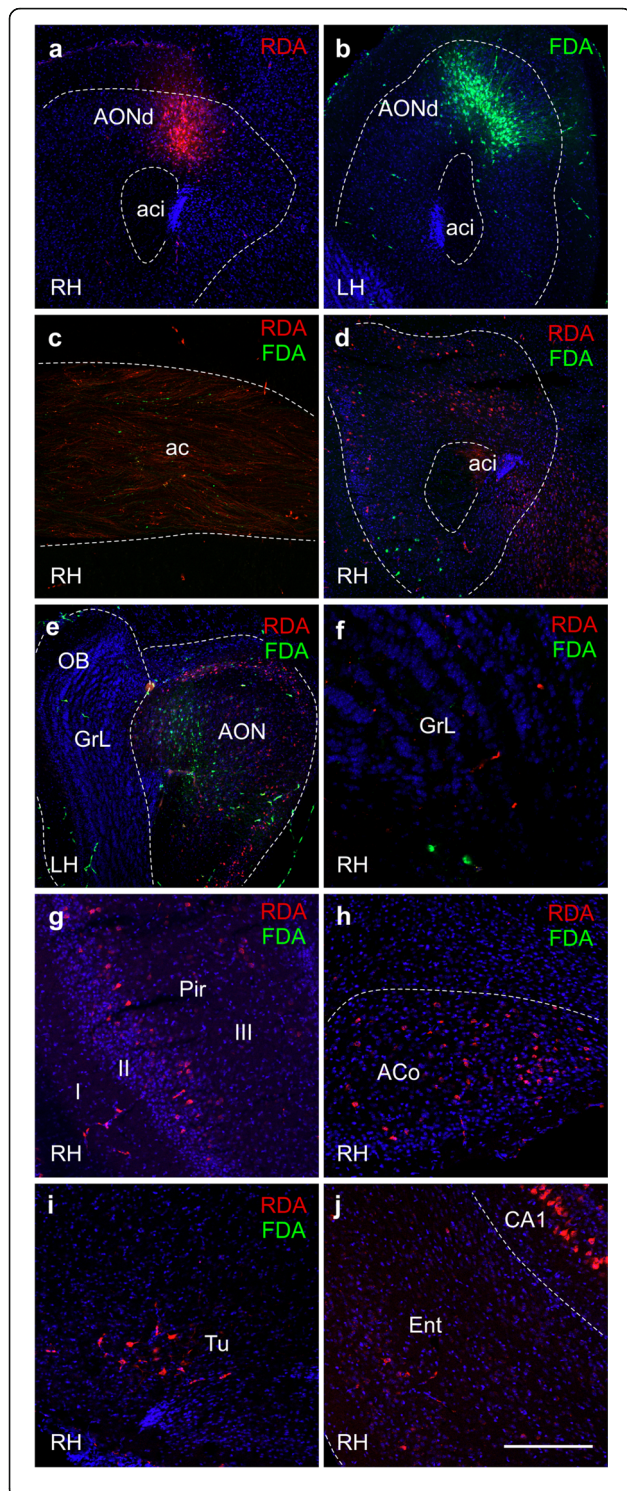


Fig. 2 RDA and FDA tracers and DAPI counterstaining. Stereotaxic coordinates were anterior 2.8; lateral 1 and depth -2.7, from dura mater. **a** RDA injection site in AONd in the right hemisphere. **b** FDA injection site in AONd in the left hemisphere. **c** Interhemispheric fibers were marked by FDA and RDA in the anterior commissure. **d** Example of ipsilateral RDA labeling and contralateral FDA labeling in right AON. **e** Example of ipsilateral FDA labeling and contralateral RDA labeling in left AON. **f** Example of ipsilateral RDA labeling and contralateral FDA labeling in right OB. Most of contralateral labeling from AONd was restricted to ventral regions of AON and closer regions of the granule cell layer (GrL) of the olfactory bulb. Images **g**, **h**, **i** and **j** show usual retrograde ipsilateral labeling in Pir, ACo, Tu and Ent (including pyramidal cells of CA1), respectively. Scale bar: **a**, **b**, **d** and **e** = 400 μ m, **c**, **g**-**j** = 200 μ m and **f** = 100 μ m. For abbreviations, see list

Genotype effect: $F(1, 64) = 39.07$, $P < 0.0001$. (Fig. 1b). However, no changes were noticed in WT mice as a function of post-injection time (Interaction: $F(3, 86) = 0.4156$, $P = 0.7420$; Treatment effect: $F(3, 86) = 1.975$, $P = 0.1237$; Time effect: $F(1, 86) = 0.4801$, $P = 0.4902$) (Fig. 1b).

Tract-tracing experiments

In order to have our own material available to analyze the AON connections, RDA and FDA were injected in the right (Fig. 2a) and left (Fig. 2b) dorsal parts of the AON, respectively. This way, ipsi- and contralateral projections could be easily compared. Axons decussate through the anterior commissure (Fig. 2c). The AON is a secondary olfactory structure and connects to the contralateral AON (Fig. 2d, e). It also connects bilaterally with primary olfactory structures, such as the OB (Fig. 2f) and, more frequently, ipsilaterally with other secondary olfactory structures such as the Pir (Fig. 2g), the anterior cortical amygdala (Fig. 2h), the olfactory tubercle (Fig. 2i) and the entorhinal cortex and hippocampus (Fig. 2j).

Immunohistochemical analysis

α -Synuclein

Immunohistochemistry against human α -synuclein revealed both exogenously injected as well as that endogenously overexpressed in TG mice. Endogenous or exogenous α -synuclein cannot be distinguished immunohistochemically. In TG animals, basal α -synuclein expression was observed after saline injection being lower in the RH (Fig. 3a, b) as compared to the LH (Fig. 3c, d). This difference was statistically significant (Fig. 4a, b). Also, in TG animals, α -synuclein injection in the RH provoked lower α -synuclein expression in the right OB (Fig. 3e, f) as compared to the left OB (Fig. 3g, h). In WT animals only the injection site is labeled (Fig. 3i, j, and dashed square in Fig. 4b).

Stereological analysis revealed variability in the α -synuclein distribution among TG groups. In the OB,

lower density was observed in saline-injected mice in the RH as opposed to the LH ($t_6 = 6.948$, $P = 0.0004$) (Fig. 4a). Interestingly, in α -synuclein-injected mice higher density was observed in the LH as compared to ipsilaterally in saline-injected mice ($t_5 = 3.805$, $P = 0.0126$) (Fig. 4a). In the AON, this trend was maintained but it was only significant between hemispheres in saline-injected animals (TG-Saline-LH vs. TG-Saline-RH: $t_6 = 3.197$, $P = 0.0187$; TG- α -LH vs. TG-Saline-LH $t_5 = 2.104$, $P = 0.0893$; TG- α -RH vs. TG-Saline-RH $t_5 = 2.310$, $P = 0.0689$) (Fig. 4b). This trend was similar but not significant in the Pir (TG-Saline-RH vs. TG- α -syn-RH: $t_5 = 2.225$, $P = 0.0767$; TG-Saline-LH vs. TG- α -syn-LH: $t_5 = 2.514$, $P = 0.0536$) (Fig. 4c) (Additional file 4: Table S8 and Figure S6).

Even though nigro-striatal projection was not the main goal of this study, histological observations were carried out to check α -synuclein direct or indirect spreading from AON to basal ganglia (caudate-putamen and substantia nigra) (Additional file 4: Figure S7 and S8). α -synuclein aggregates were mostly observed around striosomes (organization of afferent and efferent fibers in the striatum) in the caudate-putamen and substantia nigra compact part in TG animals. In addition, α -synuclein-staining appears to be more intense in α -synuclein injected TG group as compared to saline-injected TG group (Additional file 4: Figure S7 and S8). No differences between hemispheres were observed. These aggregates were not found in WT animals (Additional file 4: Figure S7 and S8).

NeuN

Neurodegeneration was evaluated by NeuN staining in OB, AON and Pir. In these areas and bilaterally, NeuN cell density (cells/mm³) was significantly higher in saline-injected WT as compared to saline-injected TG group at 2 months (OB: Kruskal-Wallis statistic 22.88, $P = 0.0018$; AON: Kruskal-Wallis statistic 20.27, $P = 0.0050$; Pir: Kruskal-Wallis statistic 23.25, $P = 0.0015$) (Table 1 and Additional file 4: Table S9). No differences between α -synuclein injected WT and TG mice were observed. In right Pir, NeuN cell density significantly decreased in α -synuclein injected WT as compared to saline-injected WT group. This trend, although not significant, was also observed in OB and AON (Table 1 and Additional file 4: Table S9).

Iba-1

Immunohistochemistry against Iba-1 showed increased labeling in the OB, specifically in the MiL in saline-injected (Fig. 5a, c) vs. α -synuclein-injected (Fig. 5b, d) TG groups. In WT animals, an abrupt reduction of labeling occurred at 4 months (Fig. 5f, h) as compared to 2 months post-injection (Fig. 5e, g). Stereological analysis was applied to the different layers of the OB (GL, EPL,

MiL, IPL, GrL), AON and Pir and it was included in Table 2 and Additional file 4: Tables S10-S13. Focusing on RH, Iba-1 density showed no differences in the different layers of OB, AON or Pir, except in MiL. In MiL, saline-injected TG mice had increased Iba-1 density as compared to α -synuclein-injected TG ($t_5 = 3.410$; $P = 0.0190$). Also, α -synuclein-injected WT mice showed higher density than α -synuclein-injected TG mice (Interaction: $F(1, 11) = 4.943$, $P = 0.0481$; Treatment effect: $F(1, 11) = 0.8695$, $P = 0.3711$; Genotype effect: $F(1, 11) = 4.519$, $P = 0.0570$). This trend was similar in the LH, revealing a reduction in α -synuclein-injected TG mice as compared to saline-injected TG in MiL ($t_5 = 3.626$; $P = 0.0151$) and Pir ($t_5 = 2.620$; $P = 0.0471$). In the WT group, post-injection time provoked an abrupt reduction of Iba-1 labeling. There are no differences between hemispheres, whereas lower levels of Iba-1 density were observed in all injected animals (saline or α -synuclein) at 4 months (GL: Interaction: $F(3, 26) = 1.253$, $P = 0.3108$; Treatment \times Time effect: $F(3, 26) = 52.42$, $P < 0.0001$; Hemisphere effect: $F(1, 26) = 0.01173$, $P = 0.9146$. EPL: Interaction: $F(3, 26) = 1.470$, $P = 0.2456$; Treatment \times Time effect: $F(3, 26) = 82.29$, $P < 0.0001$; Hemisphere effect: $F(1, 26) = 0.2745$, $P = 0.6047$. MiL: Interaction: $F(3, 26) = 0.1273$, $P = 0.9431$; Treatment \times Time effect: $F(3, 26) = 39.19$, $P < 0.0001$; Hemisphere effect: $F(1, 26) = 0.1012$, $P = 0.7530$. IPL: Interaction: $F(3, 26) = 0.1904$, $P = 0.9020$; Treatment \times Time effect: $F(3, 26) = 36.83$, $P < 0.0001$; Hemisphere effect: $F(1, 26) = 0.05854$, $P = 0.8107$. GrL: Interaction: $F(3, 26) = 1.304$, $P = 0.2944$; Treatment \times Time effect: $F(3, 26) = 149.7$, $P < 0.0001$; Hemisphere effect: $F(1, 26) = 1.179$, $P = 0.2876$. AON: Interaction: $F(3, 26) = 1.304$, $P = 0.2944$; Treatment \times Time effect: $F(3, 26) = 149.7$, $P < 0.0001$; Hemisphere effect: $F(1, 26) = 1.179$, $P = 0.2876$. Pir: Interaction: $F(3, 26) = 0.06495$, $P = 0.9779$; Treatment \times Time effect: $F(3, 26) = 35.75$, $P < 0.0001$; Hemisphere effect: $F(1, 26) = 0.001407$, $P = 0.9704$). Moreover, all injected animals showed no differences between hemispheres in the TG group as well as in WT mice (Table 2, Additional file 4: Tables S10–S13 and Figure S6).

GFAP

GFAP immunohistochemistry revealed astroglial morphology in the different layers of the OB (Fig. 6a–d), AON (Fig. 6f–i) and Pir (Fig. 6k–n) in the different experimental groups. The complex morphology of GFAP-positive cells has led us to use area fraction instead of stereological analysis for quantification. Two-way ANOVA and two-tailed t-test showed significantly higher GFAP area fraction in all injected TG (saline and α -synuclein) as compared to all WT in the right OB (Fig. 6e) (Interaction: $F(1, 11) = 0.2590$, $P = 0.6208$; Treatment effect: F

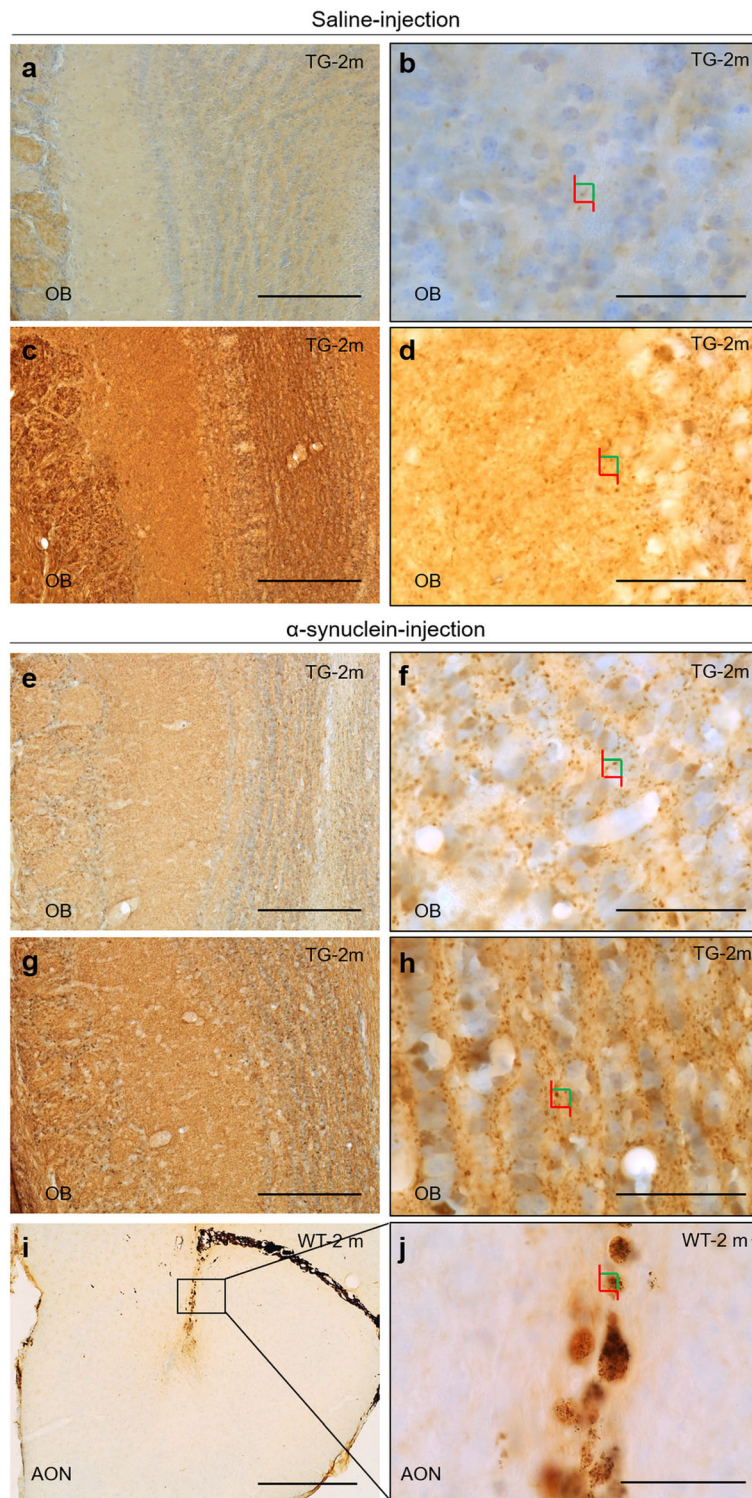


Fig. 3 Immunohistochemistry of α -synuclein aggregates in coronal sections of OB (**a-h**) and AON (**i, j**). Images **b, d, f, h** and **j** are high-magnification of images **a, c, e, g** and **i**, respectively. Colors squares indicate how stereological quantification of aggregates has been performed using optical dissector as shown in Fig. 4. Focusing on saline-injected TG, α -synuclein aggregates were decreased in RH (**a, b**) as compared to LH (**c, d**). In comparison, α -synuclein injection gave rise higher number of aggregates in RH (**e, f**) and particularly in LH (**g, h**). In WT, α -synuclein injection was only observed in AON (**i, j**). Scale bar **a, c, e, g**: 250 μ m; **b, d, f, h-j**: 50 μ m. For abbreviations, see list

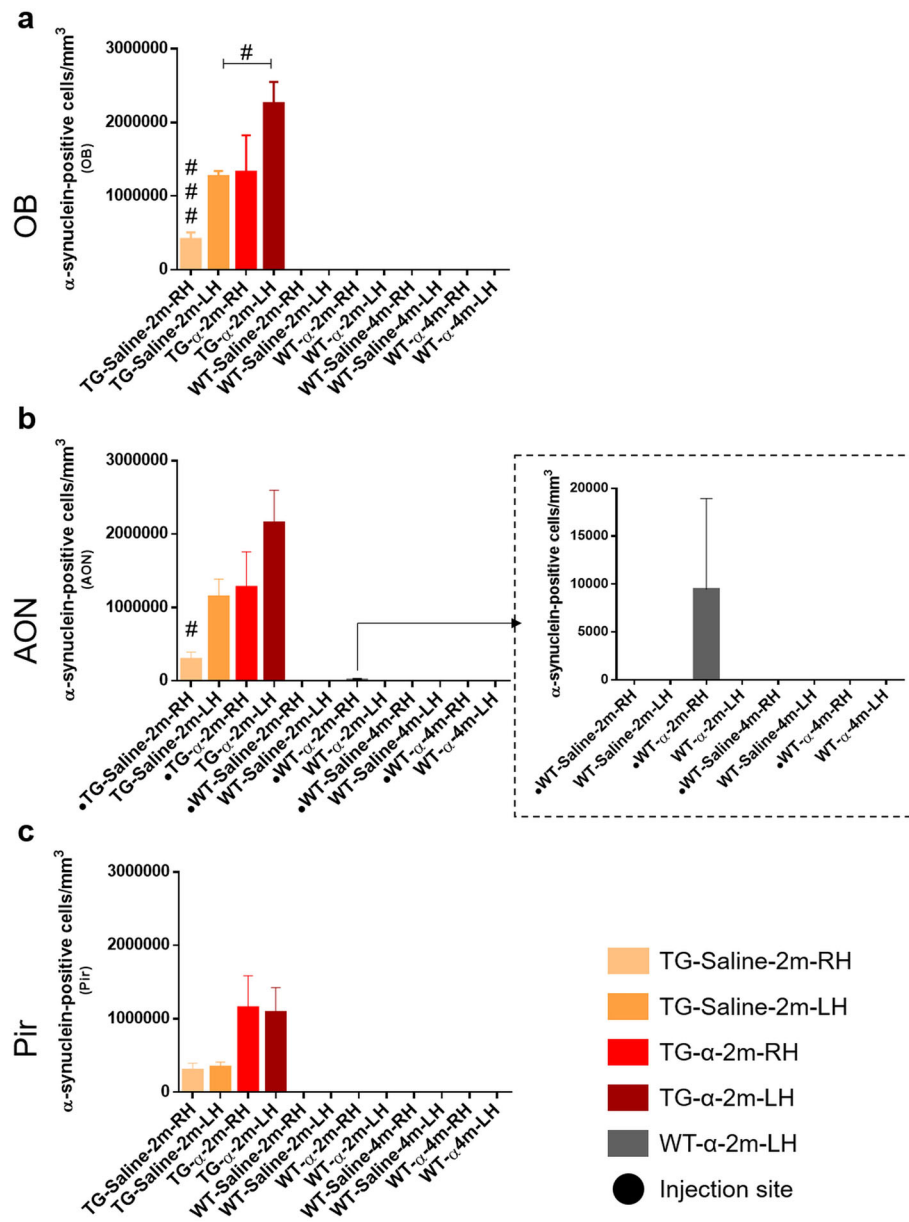


Fig. 4 Unbiased stereological quantification of α -synuclein. Graphs (mean \pm SEM) represent α -synuclein-positive cells/mm³ in OB (a), AON (b) and Pir (c). In graph b, arrow indicates counted aggregates in WT, which were only observed in the α -synuclein injection site (dashed square). T-test differences were regarded as statistically significant at # $P < 0.05$ and ### $P < 0.001$. For statistical data, see Additional file 4: Table S8. For abbreviations, see list

(1, 11) = 0.6954, $P = 0.4221$; Genotype effect: $F(1, 11) = 32.13$, $P = 0.0001$, and AON (Fig. 6j) (Interaction: $F(1, 11) = 1.121$, $P = 0.3123$; Treatment effect: $F(1, 11) = 3.740$, $P = 0.0793$; Genotype effect: $F(1, 11) = 11.73$, $P = 0.0057$. $t_6 = 3.134$; $P = 0.0202$). However, the genotype effect was maintained in AON (Fig. 6j) (Interaction: $F(1, 11) = 0.8663$, $P = 0.3720$; Treatment effect: $F(1, 11) = 0.03401$, $P = 0.8570$; Genotype effect: $F(1, 11) = 30.14$, $P = 0.0002$) and OB (Fig. 6e) (Interaction: $F(1, 11) = 0.9921$, $P = 0.3406$; Treatment effect: $F(1, 11) =$

0.08698, $P = 0.7735$; Genotype effect: $F(1, 11) = 22.10$, $P = 0.0006$) except in α -synuclein-injected TG mice in OB in the LH. No differences were observed in Pir (Fig. 6o). Focusing on WT groups, α -synuclein-injected animals showed a significant GFAP area fraction reduction in left OB (Fig. 6e) (Interaction: $F(3, 26) = 0.2841$, $P = 0.8364$; Treatment effect: $F(3, 26) = 4.233$, $P = 0.0146$; Hemisphere effect: $F(1, 26) = 1.315$, $P = 0.2619$) and Pir (Fig. 6o) (Interaction: $F(3, 26) = 1.279$, $P = 0.3024$; Treatment effect: $F(3, 26) = 2.273$, $P = 0.1038$;

Table 1 Unbiased stereological quantification of NeuN. Mean \pm SEM represent NeuN-positive cells/mm³ in the OB, AON and Pir. Statistical analysis was carried out by Kruskal-Wallis and Mann-Whitney tests. For statistical data, see Additional file 4: Table S9. For abbreviations, see list

Brain region	Genotype	Right hemisphere		Left hemisphere	
		Treatment		Treatment	
		Saline-injection	α -synuclein-injection	Saline-injection	α -synuclein-injection
OB	WT	28,894 \pm 2616	31,212 \pm 1786	34,075 \pm 2754	26,836 \pm 928.6
	TG	14,729 \pm 7364	25,604 \pm 1137	17,811 \pm 2418	24,450 \pm 698.7
AON	WT	19,728 \pm 1870	21,405 \pm 1990	22,652 \pm 2891	21,483 \pm 1725
	TG	11,197 \pm 1111	17,537 \pm 2632	11,680 \pm 1329	16,185 \pm 722.8
Pir	WT	17,451 \pm 501.7	12,642 \pm 1001	14,131 \pm 13.44	13,375 \pm 754.3
	TG	7753 \pm 155.8	12,044 \pm 778.7	8739 \pm 526.3	11,996 \pm 588.7

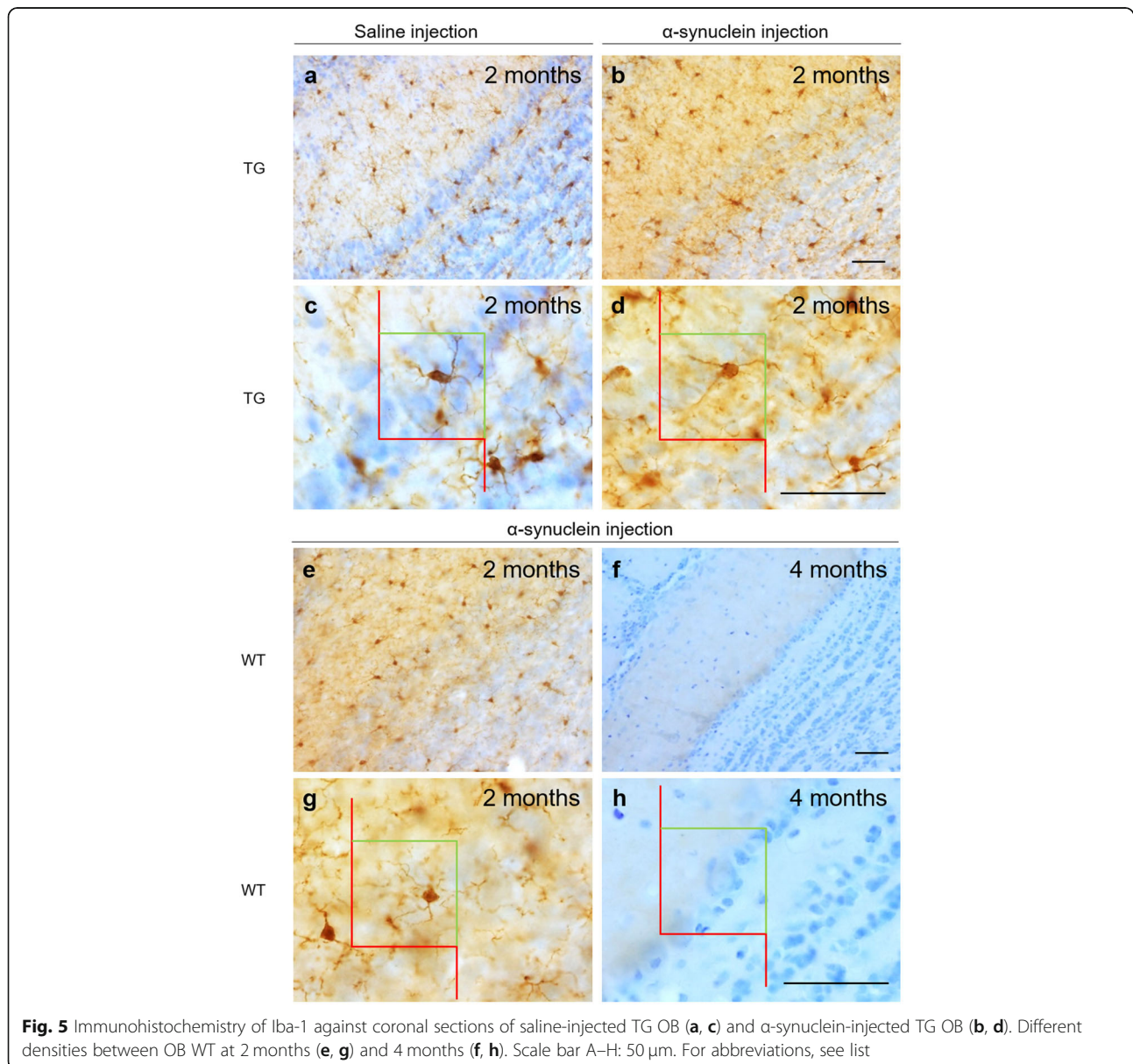


Fig. 5 Immunohistochemistry of Iba-1 against coronal sections of saline-injected TG OB (a, c) and α -synuclein-injected TG OB (b, d). Different densities between OB WT at 2 months (e, g) and 4 months (f, h). Scale bar A–H: 50 μ m. For abbreviations, see list

Table 2 Unbiased stereological quantification of Iba-1. Mean \pm SEM represent Iba-1-positive cells/mm³ in the OB layers, AON and Pir. Statistical analysis was focused on comparisons: genotype in the right hemisphere, left hemisphere, interhemispheric differences in WT and TG. For statistical data, see Additional file 4: Tables S10–S13. For abbreviations, see list

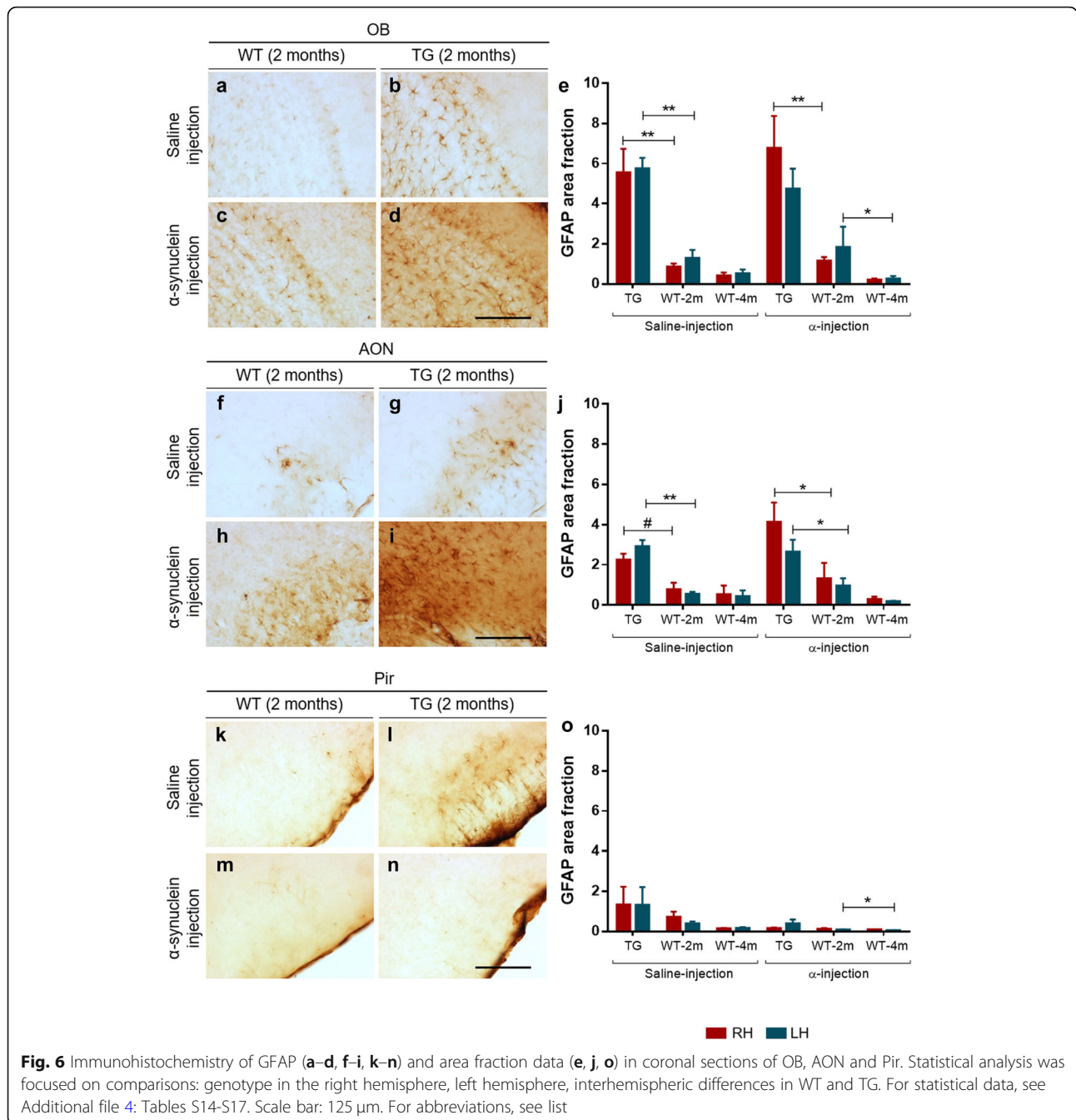
Iba-1 positive cells (cells/mm ³)						
Brain region	Genotype	Post-injection time	Right hemisphere		Left hemisphere	
			Treatment		Treatment	
			Saline-injection	α -synuclein-injection	Saline-injection	α -synuclein-injection
GL	WT	2 m	8600 \pm 475	9726 \pm 1253	10,463 \pm 931	8519 \pm 1543
		4 m	1359 \pm 199.1	3028 \pm 618.1	856 \pm 348.1	2617 \pm 613.9
	TG	2 m	7583 \pm 778.3	9249 \pm 2388	7860 \pm 548	10,569 \pm 1451
		4 m	833.4 \pm 124.5	1086 \pm 234.2	639.5 \pm 303.8	1613 \pm 582.3
EPL	WT	2 m	8260 \pm 1297	9412 \pm 538.3	8828 \pm 594.3	7514 \pm 1019
		4 m	833.4 \pm 124.5	1086 \pm 234.2	639.5 \pm 303.8	1613 \pm 582.3
	TG	2 m	7421 \pm 782	8102 \pm 482	7543 \pm 531	6762 \pm 544
		4 m	833.4 \pm 124.5	1086 \pm 234.2	639.5 \pm 303.8	1613 \pm 582.3
Mil	WT	2 m	8939 \pm 2174	10,807 \pm 1040	8921 \pm 1831	9984 \pm 1285
		4 m	935.6 \pm 449.1	1162 \pm 289.6	314.3 \pm 98.62	1599 \pm 642.4
	TG	2 m	9080 \pm 521	4513 \pm 1421	10,296 \pm 549	6338 \pm 1048
		4 m	833.4 \pm 124.5	1086 \pm 234.2	639.5 \pm 303.8	1613 \pm 582.3
IPL	WT	2 m	12,870 \pm 3512	11,089 \pm 1404	13,703 \pm 279.3	10,294 \pm 1572
		4 m	1134 \pm 402.8	1066 \pm 306.5	948.7 \pm 481.7	2209 \pm 1070
	TG	2 m	14,126 \pm 1671	8969 \pm 4074	12,480 \pm 2987	9101 \pm 3479
		4 m	833.4 \pm 124.5	1086 \pm 234.2	639.5 \pm 303.8	1613 \pm 582.3
GrL	WT	2 m	9897 \pm 361.6	10,597 \pm 733.6	10,044 \pm 321.80	8839 \pm 1185
		4 m	827.8 \pm 230.5	1301 \pm 364.3	265.6 \pm 62.71	1659 \pm 662.9
	TG	2 m	8646 \pm 876	11,231 \pm 1751	9316 \pm 934	10,632 \pm 567
		4 m	833.4 \pm 124.5	1086 \pm 234.2	639.5 \pm 303.8	1613 \pm 582.3
AON	WT	2 m	10,536 \pm 1506	10,687 \pm 2337	10,031 \pm 1196	8168 \pm 1690
		4 m	700.3 \pm 425.8	555.7 \pm 385.8	0 \pm 0	321.1 \pm 230.7
	TG	2 m	8665 \pm 1015	8084 \pm 2493	8810 \pm 703	9251 \pm 1681
		4 m	833.4 \pm 124.5	1086 \pm 234.2	639.5 \pm 303.8	1613 \pm 582.3
Pir	WT	2 m	8202 \pm 1371	8798 \pm 1763	8395 \pm 471.5	8241 \pm 2339
		4 m	108 \pm 74.58	330.7 \pm 143.7	0 \pm 0	684.8 \pm 569.9
	TG	2 m	7151 \pm 882	9312 \pm 1061	9025 \pm 546	6999 \pm 507

Hemisphere effect: $F(1, 26) = 0.6240$, $P = 0.4367$ at 4 months but not in AON (Fig. 6j). Finally, there were no differences in TG groups when comparing hemispheres (Fig. 6e, j, o) (Additional file 4: Tables S14–S17 and Figure S6).

Discussion

This study analyzes behavioral changes, connectional seeding, spreading, neuronal and glial involvement after α -synuclein injections in the right AON of TG and WT mice. Behavioral analysis reveals, in general, higher levels of hyperactivity and better motor coordination in TG as compared to WT mice (Additional file 2). Brain volume analysis detects multiple changes across the experimental groups, but no clear trend could be extrapolated (Additional file 3: Tables S3–S7). Tract-tracing experiments show that the main afferent contralateral projections to the AONd come from the AON and secondarily from the OB (Fig. 2). Regarding synucleinopathy in TG mice, two main conclusions were reached: first, in saline-injected animals, α -synuclein expression in

OB and AON is higher in LH as compared to RH, which can be attributable to basal interhemispheric differences; second, in the OB, α -synuclein injection appears to induce a significant increase in the LH as compared to saline-injected animals, which can be due to retrograde, contralateral, hodological α -synucleinopathy induction (Figs. 3 and 4). Neurodegeneration, estimated by the number of NeuN-positive cells/mm³, is observed in saline-injected TG animals as compared to saline-injected WT group at 2 months. In Pir, NeuN-positive cells/mm³ decrease in α -injected WT vs. saline-injected WT group (Table 1 and Additional file 4: Table S9). Changes observed in microglia can be attributed to the effect of the injection (Fig. 5, Table 2 and Additional file 4: Tables S10–S13). Finally, astroglia increase in TG mice independently of experimental conditions likely provoked by endogenous α -synucleinopathy, whereas in WT the α -synuclein injection provokes astrogliosis that is reverted at 4 months post-injection (Fig. 6 and Additional file 4: Tables S14–S17). Therefore, this study suggests α -synucleinopathy induction along known pathways, particularly via



retrograde transport and through contralateral projections, within the olfactory system of transgenic animals.

Connections of the anterior olfactory nucleus

The AON is preferentially involved in proteinopathies at an early stage, not only in PD [2, 15, 72, 76, 80], but also in Alzheimer’s disease [68], and it has been hypothesized that this is due to its multiple connections [67, 79]. The human AON is a structure composed of several subdivisions [77], whose connections are only inferred in the

human brain from comparative data [79], which is scarce in primates [54] but more abundant in rodents [9, 53]. The results presented here (Fig. 2) confirm that the AON is a secondary bulbar structure, reciprocally and bilaterally connected to other secondary olfactory structures, and also to at least 27 non-olfactory structures [9]. Ipsilaterally, the AON is reciprocally connected to the OB [53] (Fig. 2). Contralaterally, afferent projections to the AON are mainly originated in the AON and secondarily in the OB (Fig. 2). Accordingly, contralateral

and trans-synaptic involvement or related connections should be considered in our α -synucleinopathy results. Spreading from AON to basal ganglia, including substantia nigra and caudate-putamen, cannot be discarded via indirect pathways [79].

α -Synuclein

In order to evaluate α -synuclein spreading along the olfactory anatomical pathways [79], α -synuclein or saline were injected into the right AON. In fact, this nucleus was chosen because it could be the starting point for spreading the pathology in the brain. Actually, although analyzing nigro-striatal projection involvement was not the main objective of the study, exciting findings were reached (Additional file 4: Figure S7 and S8). Our observations confirmed that α -synucleinopathy was present in caudate-putamen and, in contrast to the original description of A53T mouse model, also in the substantia nigra [24]. Interestingly, this α -synucleinopathy in A53T model appears to be enhanced by α -synuclein injection. These aggregates were not found in WT animals (Additional file 4: Figure S7 and S8).

Although multiple studies have injected different kinds of α -synuclein in mice (preformed fibrils, oligomers, human extracts and sick mice extracts), those focused on OB/AON injections are scarce [51, 63, 64, 74]. On the other hand, A53T is a useful α -synucleinopathy model that expresses α -synuclein in olfactory structures. Previous reports of our work describe maximum synucleinopathy levels over 40 weeks [20, 21, 78, 80]. As far as we know, the present report is the first to include injections restricted to the AON in both WT and TG mice. Our results show that α -synuclein aggregates were mostly found in the contralateral hemisphere (left OB and AON) after saline injections, which could be attributable to basal interhemispheric differences (Fig. 4). This observation is very relevant in the context of unresolved motor asymmetry reported in PD [16]. Another interesting observation is that there is a trend for a denser labeling in the contralateral hemisphere of α -synuclein-injected TG as compared to saline-injected TG animals, particularly in the OB (Fig. 4). This could be related to the previously described contralateral projections (Fig. 2), indicating α -synucleinopathy retrograde induction (seeding and/or spreading). Endogenous α -synuclein expressed in TG animals would be necessary to allow exogenous injected α -synuclein to increase synucleinopathy in the contralateral hemisphere. Thus, we suggest that exogenous α -synuclein is able to induce seeding and/or spreading to the contralateral hemisphere in TG animals. In WT animals, α -synuclein was only detected at the injection site. These results could be due to different factors: susceptibility to a prior seeding, time-dependent spreading or reactivity of different molecular α -synuclein

species. First, it has been reported that α -synuclein preformed fibrils-inoculated A53T mice enhanced the conversion of endogenous α -synuclein into pathological forms, acting as a template. This has been reported not only in vivo, but also in vitro, since α -synuclein aggregation could occur as a nucleation-dependent mechanism [48]. Second, the post-injection periods vary in different studies, ranging from 72 h to 30, 90 or 180 days [48, 64, 66]. Third, despite α -synuclein oligomerizing and aggregating into fibrils under pathological conditions, it has been reported that monomers and oligomers were more rapidly transferred from OB of WT to interconnected regions as compared to fibrils [64]. Therefore, it would be interesting to have this kind of molecule available to improve the injection results; α -synuclein recombinants are larger, which possibly makes spreading more difficult, thus requiring more time. In agreement with our results, α -synuclein fibrils have been intrahippocampally injected in TG and WT mice, without α -synuclein spread from the injection site having been detected in WT after 2 months [66].

NeuN

PD is characterized by neurodegeneration of dopaminergic neurons in the substantia nigra pars compacta and the corresponding denervation in the striatum [39]. Interestingly, in patients, this has been correlated with neuronal loss in the OB [35].

Neurodegeneration has been checked using NeuN labeling in different mouse PD models, including 6-OHDA injections [46], adeno-associated-virus vector (AAV9) for α -synuclein [57] and transgenic mouse overexpressing human α -synuclein under the Thy-1 promoter (Thy- α -syn) [11]. Bilaterally, in OB, AON and Pir, our results showed that the number of NeuN-positive cells/mm³ (density) was higher in saline-injected WT group as compared to saline-injected TG mice at 2 months. Given that these differences are not observed in α -synuclein injected animals, we suggested that, in WT mice, α -synuclein injection might be also involved in neurodegeneration. In fact, in Pir, NeuN density decreased in α -synuclein injected WT as compared to saline-injected WT group.

No differences were noticed in TG animals, regardless of injection and hemispheres. It could be due to the fact that A53T mouse model constitutively expresses human α -synuclein gene, therefore α -synuclein injection could provoke minor induction on neurodegeneration. As far as we know, this is the first report describing unbiased NeuN counting in olfactory structures in A53T mouse model.

Regarding α -synucleinopathy and neurodegeneration, despite of our results show basal interhemispheric differences in α -synuclein aggregates in saline-injected TG in

OB and AON, there is not correlation to neuronal loss. Likewise, although data show an increase of α -synuclein between saline-injected TG and α -synuclein-injected TG in left OB, no differences were observed in NeuN counting.

The density of NeuN differences between saline-injection TG and saline-injection WT could be due to transgene. These differences disappeared in α -synuclein injected animals. So, it could be as a consequence of exogenous α -synuclein inoculation. In WT mice, although our findings indicated that α -synuclein was restricted to the injection site (right AON), neuronal loss was significantly observed in Pir. It could be due to the fact that our α -synuclein antibody is able to label α -synuclein aggregates but no other conformations such as fibrils or soluble forms, which could act on neurodegeneration as well.

Glial markers

Both microglia and astroglia have been involved in PD progression [32] and associated α -synucleinopathy [7].

Microglia

Microglia are actively involved both in healthy brains and in different neurodegenerative disorders such as Parkinson's and Alzheimer's diseases [69]. Microglia play multiple roles in neuronal survival, not only in physiological inflammatory responses but also in non-inflammatory ones. For example, their involvement in homeostasis, programmed cell death and clearance of apoptotic newborn neurons has been reported, as well as synaptic pruning and synaptic plasticity [69]. Focusing on PD, neuroinflammation has been described not only as a consequence of neurodegeneration, but also as an issue at the onset of this disease [45]. As previous studies have shown that the brains of PD patients have extensive microglial activation [45], one of the aims of this study was to quantify microglia (Iba-1-positive cells) in an A53T mouse model and WT mice to detect microgliosis after saline or α -synuclein injections. Surprisingly, our results only showed a reduction of Iba-1-positive cells in α -synuclein-injected TG mice as compared to saline-injected TG or α -synuclein-injected WT in the MiL and Pir (Fig. 5 and Table 2). This might be due to the fact that TG mice have endogenous human α -synuclein and, as we injected with a similar molecular species, it was not detected as exogenous. On the other hand, our results have shown a significant time-dependent decrease after 4 months in WT (Fig. 5 and Table 2). Thereby, the injection/surgery might have triggered a small amount of microgliosis. The effect of microgliosis in PD remains controversial because it can be both beneficial and detrimental [45]. In addition, we assessed differences in microglial morphology (larger cell bodies and shorter and thicker dendrites) that were correlated to the detection of homeostatic changes (image not shown).

Astroglia

Astrocytes are the largest cells in the brain. Their critical functions include maintaining a homeostatic microenvironment (modulating oxidative stress and regulating glucose metabolism), neuronal survival, neurotransmission and injury repair, among others [32, 37]. Interestingly, it has been proposed that astrocytes can establish communications with neurons, microglia and other astrocytes. In fact, it has been suggested that one of the likely causes of neuronal death could be astrocyte dysfunction [37] and also that activated astrocytes can prevent neuronal death. Indeed, published reports indicate that PD genes are expressed in both astrocytes and microglia, and that astrogliosis is activated in PD. Astroglia protect neurons from oxidative stress and inhibit excessive inflammation by regulating microglial activation. Taking all this into consideration, one of the aims of this study was to evaluate the GFAP area fraction in all injected animals. Our results indicated that the GFAP area fraction increased in all injected TG (saline or α -synuclein) as compared to all WT in the right OB and AON (Fig. 6e, j). In agreement with these results, non-injected TG mice showed a higher number of GFAP-positive cells in the striatum and substantia nigra as compared to WT [73]. However, the GFAP area fraction decreased at 4 months in WT mice (Fig. 6e, j, o). Therefore, injection/surgery could have triggered astrogliosis as well as microgliosis in WT mice.

Conclusions

Being aware of limitations of study due to lethality, the main conclusions reached are the followings. In TG saline-injected animals, α -synuclein expression in OB and AON is higher in LH as compared to RH (Fig. 4 a and b); and, in the OB, α -synuclein injection could provoke a significant increase in the LH as compared to saline-injected animals (Fig. 4a). This study suggests connectional seeding and/or spreading of α -synuclein along known olfactory pathways of TG animals, particularly via retrograde transport and through AON to the contralateral OB (Fig. 2). Neurodegeneration might be correlated with transgene and exogenous α -synuclein inoculation could induce neuronal loss in WT animals, even though this α -synucleinopathy cannot be detected (Table 1 and Additional file 4). Microglia labeling was apparently correlated with surgery-induced inflammation (Fig. 5, Table 2 and Additional file 4). On the other hand, astroglial labeling was higher in TG animals, which could be due to endogenous α -synucleinopathy; whereas in WT the α -synuclein injection could provoke astrogliosis that is reverted at 4 months post-injection (Fig. 6 and Additional file 4). Behavioral changes observed might be mostly attributable to genotype (Additional file 2).

Additional files

Additional file 1: Material and methods. **Table S1.** Antibodies. **Table S2.** Parameters of unbiased, design-based stereology. (PDF 123 kb)

Additional file 2: Behavioral analyses. **Figure S1.** Corner test. **Figure S2.** Open field test. **Figure S3** Rotarod test. **Figure S4.** Wire hang test. (PDF 948 kb)

Additional file 3: Brain volume. **Table S3.** Brain volume. **Table S4.** Volume statistical data. Comparison of genotype in the right hemisphere. **Table S5.** Volume statistical data. Comparison of genotype in the left hemisphere. **Table S6.** Volume statistical data. Comparison of hemispheres in WT. **Table S7.** Volume statistical data. Comparison of hemispheres in TG. **Figure S5.** OB and AON volume 3D model. (PDF 233 kb)

Additional file 4: Stereological α -synuclein, NeuN, Iba-1 and GFAP quantification. **Table S8.** Statistical data of stereological α -synuclein quantification. **Table S9.** Statistical data of NeuN quantification (Mann-Whitney test). **Table S10.** Statistical data of stereological Iba-1 quantification. Comparison of genotype in the right hemisphere. **Table S11.** Statistical data of stereological Iba-1 quantification. Comparison of genotype in the left hemisphere. **Table S12.** Statistical data of stereological Iba-1 quantification. Comparison of hemispheres in WT. **Table S13.** Statistical data of stereological Iba-1 quantification. Comparison of hemispheres in TG. **Table S14.** Statistical data of GFAP quantification. Comparison of genotype in the right hemisphere. **Table S15.** Statistical data of GFAP quantification. Comparison of genotype in the left hemisphere. **Table S16.** Statistical data of GFAP quantification. Comparison of hemispheres in WT. **Table S17.** Statistical data of GFAP quantification. Comparison of hemispheres in TG. **Figure S6.** AON injection site labeled with different markers. **Figure S7.** α -synucleinopathy in caudate-putamen. **Figure S8.** α -synucleinopathy in substantia nigra. (PDF 814 kb)

Abbreviations

ABC: Avidin-biotin complex; ac: Anterior commissure; aci: Anterior commissure intrabulbar; ACo: Anterior cortical amygdala; AOD: Anterior olfactory area dorsal part; AOL: Anterior olfactory area lateral part; AOM: Anterior olfactory area medial part; AON: Anterior olfactory nucleus; AONd: Dorsal anterior olfactory nucleus; AOV: Anterior olfactory area ventral part; CA1: Field CA1 of Ammon's horn; Ent: Entorhinal cortex; EPL: External plexiform layer; FDA: Fluorescein-labeled dextran amine; g: Grams; GFAP: Glial fibrillary acidic protein; GL: Glomerular layer; GrL: Granule cell layer; Iba-1: Ionized calcium binding adaptor molecule 1; IH: Interhemispheric; IHC: Immunohistochemistry; IPL: Internal plexiform layer; LH: Left hemisphere; m: Months; Mil: Mitral cell layer; mm: Millimeter; OB: Olfactory bulb; PBS: Phosphate-buffered saline; PD: Parkinson's disease; Pir: Piriform cortex; RDA: Rhodamine-labeled dextran amine; RH: Right hemisphere; rpm: Revolutions per minute; S: Saline solution; s: Seconds; SNC: Substantia nigra, compact part; SNR: Substantia nigra, reticular part; TG: Transgenic; Tu: Olfactory tubercle; WT: Wild-type; α : α -synuclein; α -syn: α -synuclein

Acknowledgements

This study was supported by the Spanish Ministry of Economy and Competitiveness-FEDER (grant # SAF2016-75768-R) and the Autonomous Government of Castilla-La Mancha/FEDER (grant no. SBPLY/17/180501/000430). The authors would like to thank Lydia Gimenez-Llort for behavioral test advice. We thank Sara Fairén and Calum Ross for the English edition of this manuscript.

Funding

Sponsored by the Spanish Ministry of Economy and Competitiveness-FEDER (grant # SAF2016-75768-R) to AMM and the Autonomous Government of Castilla-La Mancha/FEDER (grant no. SBPLY/17/180501/000430) to AMM and DSS.

Availability of data and materials

The datasets used and/or analyzed during the current study are available from the corresponding author on reasonable request.

Authors' contributions

Study design: IUB, AFC, DSS, AMM, AMM. Behavioral analysis: IUB, AFC. Tissue section: IUB, AFC, DSS. Immunohistochemistry: IUB, AFC. Image capture: IUB, DSS. Data analysis: IUB, AFC, AMM. Discussion and writing: AFC, DSS, AMM, AMM, IUB. All authors read and approved the final manuscript.

Ethics approval and consent to participate

All experiments carried out were in agreement with European (Directive 2010/63/EU) and Spanish (RD 53/2013) regulations on the protection of animals used for scientific purposes, and they were also approved by the Ethical Committee for Animal Research of the University of Castilla-La Mancha (SAF2016-75768-R).

Consent for publication

All the authors have approved publication.

Competing interests

The authors declare that they have no competing interests.

Publisher's Note

Springer Nature remains neutral with regard to jurisdictional claims in published maps and institutional affiliations.

Author details

¹Neuroplasticity and Neurodegeneration Laboratory, CRIB, Ciudad Real Medical School, University of Castilla-La Mancha, Camino de Moledores s/n, Ciudad Real 13071, Spain. ²School of Occupational Therapy, Speech Therapy and Nursing, University of Castilla-La Mancha, Talavera de la Reina, Spain.

Received: 7 February 2019 Accepted: 1 April 2019

Published online: 15 April 2019

References

1. Aboutit S, Bousset L, Loria F, Zhu S, de Chaumont F, Pieri L, Olivo-Marin JC, Melki R, Zurzolo C (2016) Tunneling nanotubes spread fibrillar alpha-synuclein by intercellular trafficking of lysosomes. *EMBO J* 35(19):2120–2138
2. Attems J, Walker L, Jellinger KA (2014) Olfactory bulb involvement in neurodegenerative diseases. *Acta Neuropathol* 127(4):459–475
3. Baeta-Corral R, Gimenez-Llort L (2014) Bizarre behaviors and risk assessment in 3xTg-AD mice at early stages of the disease. *Behav Brain Res* 258:97–105
4. Beach TG, White CL 3rd, Hladik CL, Sabbagh MN, Connor DJ, Shill HA, Sue LI, Sasse J, Bachalakuri J, Henry-Watson J, Akiyama H, Adler CH, Arizona Parkinson's Disease C (2009) Olfactory bulb alpha-synucleinopathy has high specificity and sensitivity for Lewy body disorders. *Acta Neuropathol* 117(2):169–174
5. Braak H, Del Tredici K, Rub U, de Vos RA, Jansen Steur EN, Braak E (2003) Staging of brain pathology related to sporadic Parkinson's disease. *Neurobiol Aging* 24(2):197–211
6. Braak H, Sastre M, Del Tredici K (2007) Development of alpha-synuclein immunoreactive astrocytes in the forebrain parallels stages of intraneuronal pathology in sporadic Parkinson's disease. *Acta Neuropathol* 114(3):231–241
7. Bruck D, Wenning GK, Stefanova N, Fellner L (2016) Glia and alpha-synuclein in neurodegeneration: a complex interaction. *Neurobiol Dis* 85:262–274
8. Brundin P, Li JY, Holton JL, Lindvall O, Revesz T (2008) Research in motion: the enigma of Parkinson's disease pathology spread. *Nat Rev Neurosci* 9(10):741–745
9. Brunjes PC, Illig KR, Meyer EA (2005) A field guide to the anterior olfactory nucleus (cortex). *Brain Res Brain Res Rev* 50(2):305–335
10. Cavaliere F, Cerf L, Dehay B, Ramos-Gonzalez P, De Giorgi F, Bourdenx M, Bessedé A, Obeso JA, Matute C, Icha S, Bezard E (2017) In vitro alpha-synuclein neurotoxicity and spreading among neurons and astrocytes using Lewy body extracts from Parkinson disease brains. *Neurobiol Dis* 103:101–112
11. Coulombe K, Kerdiles O, Tremblay C, Emond V, Lebel M, Boulianne AS, Plourde M, Cicchetti F, Calon F (2018) Impact of DHA intake in a mouse model of synucleinopathy. *Exp Neurol* 301(Pt A):39–49
12. Daniel SE, Hawkes CH (1992) Preliminary diagnosis of Parkinson's disease by olfactory bulb pathology. *Lancet* 340(8812):186
13. De Vos KJ, Grierson AJ, Ackerley S, Miller CC (2008) Role of axonal transport in neurodegenerative diseases. *Annu Rev Neurosci* 31:151–173

14. Del Tredici K, Braak H (2016) Review: sporadic Parkinson's disease: development and distribution of alpha-synuclein pathology. *Neuropathol Appl Neurobiol* 42(1):33–50
15. Del Tredici K, Rub U, De Vos RA, Bohl JR, Braak H (2002) Where does parkinson disease pathology begin in the brain? *J Neuropathol Exp Neurol* 61(5):413–426
16. Djaldetti R, Ziv I, Melamed E (2006) The mystery of motor asymmetry in Parkinson's disease. *Lancet Neurol* 5(9):796–802
17. Doty RL (2017) Olfactory dysfunction in neurodegenerative diseases: is there a common pathological substrate? *Lancet Neurol* 16(6):478–488
18. Dunning CJ, Reyes JF, Steiner JA, Brundin P (2012) Can Parkinson's disease pathology be propagated from one neuron to another? *Prog Neurobiol* 97(2):205–219
19. Ferreira SA, Romero-Ramos M (2018) Microglia response during Parkinson's Disease: alpha-Synuclein intervention. *Front Cell Neurosci* 12:247
20. Flores-Cuadrado A, Ubeda-Banon I, Saiz-Sanchez D, de la Rosa-Prieto C, Martinez-Marcos A (2015) Alpha-Synuclein staging in the amygdala of a Parkinson's disease model: cell types involved. *Eur J Neurosci* 41(1):137–146
21. Flores-Cuadrado A, Ubeda-Banon I, Saiz-Sanchez D, de la Rosa-Prieto C, Martinez-Marcos A (2016) Hippocampal alpha-synuclein and interneurons in Parkinson's disease: data from human and mouse models. *Mov Disord* 31(7):979–988
22. Franklin KBJ, Paxinos G (2008) The mouse brain in stereotaxic coordinates. Elsevier, San Diego
23. Gerhard A, Pavese N, Hotton G, Turkheimer F, Es M, Hammers A, Eggert K, Oertel W, Banati RB, Brooks DJ (2006) In vivo imaging of microglial activation with [¹¹C](R)-PK11195 PET in idiopathic Parkinson's disease. *Neurobiol Dis* 21(2):404–412
24. Giasson BI, Duda JE, Quinn SM, Zhang B, Trojanowski JQ, Lee VM (2002) Neuronal alpha-synucleinopathy with severe movement disorder in mice expressing A53T human alpha-synuclein. *Neuron* 34(4):521–533
25. Gimenez-Llort L, Fernandez-Teruel A, Escorihuela RM, Fredholm BB, Tobena A, Pekny M, Johansson B (2002) Mice lacking the adenosine A1 receptor are anxious and aggressive, but are normal learners with reduced muscle strength and survival rate. *Eur J Neurosci* 16(3):547–550
26. Glaser J, Green G, Hendricks S (2007) Stereology for biological research with a focus on neuroscience. MBF Press, Williston
27. Glass CK, Saijo K, Winner B, Marchetto MC, Gage FH (2010) Mechanisms underlying inflammation in neurodegeneration. *Cell* 140(6):918–934
28. Goedert M (2001) Alpha-synuclein and neurodegenerative diseases. *Nat Rev Neurosci* 2(7):492–501
29. Goedert M (2015) NEURODEGENERATION. Alzheimer's and Parkinson's diseases: the prion concept in relation to assembled Abeta, tau, and alpha-synuclein. *Science* 349(6248):1255–1255
30. Gu XL, Long CX, Sun L, Xie C, Lin X, Cai H (2010) Astrocytic expression of Parkinson's disease-related A53T alpha-synuclein causes neurodegeneration in mice. *Mol Brain* 3:12
31. Gutierrez-Castellanos N, Martinez-Marcos A, Martinez-Garcia F, Lanuza E (2010) Chemosensory function of the amygdala. *Vitam Horm* 83:165–196
32. Halliday GM, Stevens CH (2011) Glia: initiators and progressors of pathology in Parkinson's disease. *Mov Disord* 26(1):6–17
33. Hansen C, Li JY (2012) Beyond alpha-synuclein transfer: pathology propagation in Parkinson's disease. *Trends Mol Med* 18(5):248–255
34. Hirsch EC, Vyas S, Hunot S (2012) Neuroinflammation in Parkinson's disease. *Parkinsonism Relat Disord* 18(Suppl 1):S210–S212
35. Iacono D, Geraci-Erck M, Rabin ML, Adler CH, Serrano G, Beach TG, Kurlan R (2015) Parkinson disease and incidental Lewy body disease: just a question of time? *Neurology* 85(19):1670–1679
36. Jellinger KA (2010) Critical evaluation of the Braak staging scheme for Parkinson's disease. *Ann Neurol* 67(4):550
37. Joe EH, Choi DJ, An J, Eun JH, Jou I, Park S (2018) Astrocytes, microglia, and Parkinson's Disease. *Exp Neurobiol* 27(2):77–87
38. Jucker M, Walker LC (2013) Self-propagation of pathogenic protein aggregates in neurodegenerative diseases. *Nature* 501(7465):45–51
39. Kalia LV, Lang AE (2015) Parkinson's disease. *Lancet* 386(9996):896–912
40. Kim S, Cho SH, Kim KY, Shin KY, Kim HS, Park CH, Chang KA, Lee SH, Cho D, Suh YH (2009) Alpha-synuclein induces migration of BV-2 microglial cells by up-regulation of CD44 and MT1-MMP. *J Neurochem* 109(5):1483–1496
41. Kohl Z, Schlachetki JC, Feldewerth J, Hornauer P, Munch M, Adame A, Riemenschneider MJ, Winkler J, Masliah E (2017) Distinct pattern of microgliosis in the olfactory bulb of neurodegenerative Proteinopathies. *Neural Plast* 2017:3851262
42. Lashuel HA, Overk CR, Oueslati A, Masliah E (2013) The many faces of alpha-synuclein: from structure and toxicity to therapeutic target. *Nat Rev Neurosci* 14(1):38–48
43. Lastres-Becker I, Ulusoy A, Innamorato NG, Sahin G, Rabano A, Kirik D, Cuadrado A (2012) Alpha-Synuclein expression and Nrf2 deficiency cooperate to aggravate protein aggregation, neuronal death and inflammation in early-stage Parkinson's disease. *Hum Mol Genet* 21(14):3173–3192
44. Li JY, Englund E, Holton JL, Soulet D, Haggell P, Lees AJ, Lashley T, Quinn NP, Rehnroona S, Bjorklund A, Widner H, Revesz T, Lindvall O, Brundin P (2008) Lewy bodies in grafted neurons in subjects with Parkinson's disease suggest host-to-graft disease propagation. *Nat Med* 14(5):501–503
45. Lim S, Chun Y, Lee JS, Lee SJ (2016) Neuroinflammation in Synucleinopathies. *Brain Pathol* 26(3):404–409
46. Lima JC, Oliveira LM, Botelho MT, Moreira TS, Takakura AC (2018) The involvement of the pathway connecting the substantia nigra, the periaqueductal gray matter and the reticulospinal nucleus in breathing control in a rat model of Parkinson's disease. *Exp Neurol* 302:46–56
47. Loria F, Vargas JY, Bousset L, Syan S, Salles A, Melki R, Zurzolo C (2017) Alpha-Synuclein transfer between neurons and astrocytes indicates that astrocytes play a role in degradation rather than in spreading. *Acta Neuropathol* 134(5):789–808
48. Luk KC, Kehm V, Carroll J, Zhang B, O'Brien P, Trojanowski JQ, Lee VM (2012) Pathological alpha-synuclein transmission initiates Parkinson-like neurodegeneration in nontransgenic mice. *Science* 338(6109):949–953
49. Martin LJ (2007) Transgenic mice with human mutant genes causing Parkinson's disease and amyotrophic lateral sclerosis provide common insight into mechanisms of motor neuron selective vulnerability to degeneration. *Rev Neurosci* 18(2):115–136
50. Martinez-Marcos A (2009) On the organization of olfactory and vomeronasal cortices. *Prog Neurobiol* 87(1):21–30
51. Mason DM, Nouraei N, Pant DB, Miner KM, Hutchison DF, Luk KC, Stolz JF, Leak RK (2016) Transmission of alpha-synucleinopathy from olfactory structures deep into the temporal lobe. *Mol Neurodegener* 11(1):49
52. Masuda-Suzukake M, Nonaka T, Hosokawa M, Oikawa T, Arai T, Akiyama H, Mann DM, Hasegawa M (2013) Prion-like spreading of pathological alpha-synuclein in brain. *Brain* 136(Pt 4):1128–1138
53. Mohedano-Moriano A, de la Rosa-Prieto C, Saiz-Sanchez D, Ubeda-Banon I, Pro-Sistiaga P, de Moya-Pinilla M, Martinez-Marcos A (2012) Centrifugal telencephalic afferent connections to the main and accessory olfactory bulbs. *Front Neuroanat* 6:19
54. Mohedano-Moriano A, Martinez-Marcos A, Munoz M, Arroyo-Jimenez MM, Marcos P, Artacho-Perula E, Blaizot X, Insausti R (2005) Reciprocal connections between olfactory structures and the cortex of the rostral superior temporal sulcus in the Macaca fascicularis monkey. *Eur J Neurosci* 22(10):2503–2518
55. Oaks AW, Frankfurt M, Finkelstein DI, Sidhu A (2013) Age-dependent effects of A53T alpha-synuclein on behavior and dopaminergic function. *PLoS One* 8(4):e60378
56. Obeso JA, Stamelou M, Goetz CG, Poewe W, Lang AE, Weintraub D, Burn DJ, Halliday GM, Bezdard E, Przedborski S, Lehericy S, Brooks DJ, Rothwell JC, Hallett M, DeLong MR, Marras C, Tanner CM, Ross GW, Langston JW, Klein C, Bonifati V, Jankovic J, Lozano AM, Deuschl G, Bergman H, Tolosa E, Rodriguez-Violante M, Fahn S, Postuma RB, Berg D, Marek K, Standaert DG, Surmeier DJ, Olanow CW, Kordower JH, Calabresi P, Schapira AHV, Stoessl AJ (2017) Past, present, and future of Parkinson's disease: a special essay on the 200th anniversary of the shaking palsy. *Mov Disord* 32(9):1264–1310
57. Pabon MM, Jernberg JN, Morganti J, Contreras J, Hudson CE, Klein RL, Bickford PC (2012) A spirulina-enhanced diet provides neuroprotection in an alpha-synuclein model of Parkinson's disease. *PLoS One* 7(9):e45256
58. Paumier KL, Sukoff Rizzo SJ, Berger Z, Chen Y, Gonzales C, Kaftan E, Li L, Lotarski S, Monaghan M, Shen W, Stolyar P, Vasilyev D, Zaleska M, Hirst WD, Dunlop J (2013) Behavioral characterization of A53T mice reveals early and late stage deficits related to Parkinson's disease. *PLoS One* 8(8):e70274
59. Poewe W, Seppi K, Tanner CM, Halliday GM, Brundin P, Volkman J, Schrag AE, Lang AE (2017) Parkinson disease. *Nat Rev Dis Primers* 3:17013
60. Prusiner SB (1987a) Prions and neurodegenerative diseases. *N Engl J Med* 317(25):1571–1581
61. Prusiner SB (1987b) Prions causing degenerative neurological diseases. *Annu Rev Med* 38:381–398
62. Prusiner SB (2012) Cell biology. A unifying role for prions in neurodegenerative diseases. *Science* 336(6088):1511–1513

63. Rey NL, George S, Steiner JA, Madaj Z, Luk KC, Trojanowski JQ, Lee VM, Brundin P (2018a) Spread of aggregates after olfactory bulb injection of alpha-synuclein fibrils is associated with early neuronal loss and is reduced long term. *Acta Neuropathol* 135(1):65–83
64. Rey NL, Petit GH, Bousset L, Melki R, Brundin P (2013) Transfer of human alpha-synuclein from the olfactory bulb to interconnected brain regions in mice. *Acta Neuropathol* 126(4):555–573
65. Rey NL, Wesson DW, Brundin P (2018b) The olfactory bulb as the entry site for prion-like propagation in neurodegenerative diseases. *Neurobiol Dis* 109(Pt B):226–248
66. Sacino AN, Brooks M, McKinney AB, Thomas MA, Shaw G, Golde TE, Giasson BI (2014) Brain injection of alpha-synuclein induces multiple proteinopathies, gliosis, and a neuronal injury marker. *J Neurosci* 34(37):12368–12378
67. Saiz-Sanchez D, Flores-Cuadrado A, Ubeda-Banon I, de la Rosa-Prieto C, Martinez-Marcos A (2016) Interneurons in the human olfactory system in Alzheimer's disease. *Exp Neurol* 276:13–21
68. Saiz-Sanchez D, Ubeda-Banon I, de la Rosa-Prieto C, Argandona-Palacios L, Garcia-Munozguren S, Insausti R, Martinez-Marcos A (2010) Somatostatin, tau, and beta-amyloid within the anterior olfactory nucleus in Alzheimer disease. *Exp Neurol* 223(2):347–350
69. Salter MW, Stevens B (2017) Microglia emerge as central players in brain disease. *Nat Med* 23(9):1018–1027
70. Savica R, Bradley BF, Mielke MM (2018) When do alpha-Synucleinopathies start? An epidemiological timeline: a review. *JAMA Neurol* 75(4):503–509
71. Schapira AHV, Chaudhuri KR, Jenner P (2017) Non-motor features of Parkinson disease. *Nat Rev Neurosci* 18(8):509
72. Sengoku R, Saito Y, Ikemura M, Hatsuta H, Sakiyama Y, Kanemaru K, Arai T, Sawabe M, Tanaka N, Mochizuki H, Inoue K, Murayama S (2008) Incidence and extent of Lewy body-related alpha-synucleinopathy in aging human olfactory bulb. *J Neuropathol Exp Neurol* 67(11):1072–1083
73. Sirabella R, Sisalli MJ, Costa G, Omura K, Ianniello G, Pinna A, Morelli M, Di Renzo GM, Annunziato L, Scorziello A (2018) NCX1 and NCX3 as potential factors contributing to neurodegeneration and neuroinflammation in the A53T transgenic mouse model of Parkinson's Disease. *Cell Death Dis* 9(7):725
74. Steiner JA, Quansah E, Brundin P (2018) The concept of alpha-synuclein as a prion-like protein: ten years after. *Cell Tissue Res* 373(1):161–173
75. Stokholm MG, Iranzo A, Ostergaard K, Serradell M, Otto M, Svendsen KB, Garrido A, Vilas D, Borghammer P, Santamaria J, Moller A, Gaig C, Brooks DJ, Tolosa E, Pavese N (2017) Assessment of neuroinflammation in patients with idiopathic rapid-eye-movement sleep behaviour disorder: a case-control study. *Lancet Neurol* 16(10):789–796
76. Ubeda-Banon I, Flores-Cuadrado A, Saiz-Sanchez D, Martinez-Marcos A (2017) Differential effects of Parkinson's Disease on interneuron subtypes within the human anterior olfactory nucleus. *Front Neuroanat* 11:113
77. Ubeda-Banon I, Saiz-Sanchez D, de la Rosa-Prieto C, Argandona-Palacios L, Garcia-Munozguren S, Martinez-Marcos A (2010a) Alpha-Synucleinopathy in the human olfactory system in Parkinson's disease: involvement of calcium-binding protein- and substance P-positive cells. *Acta Neuropathol* 119(6):723–735
78. Ubeda-Banon I, Saiz-Sanchez D, de la Rosa-Prieto C, Martinez-Marcos A (2012) Alpha-Synuclein in the olfactory system of a mouse model of Parkinson's disease: correlation with olfactory projections. *Brain Struct Funct* 217(2):447–458
79. Ubeda-Banon I, Saiz-Sanchez D, de la Rosa-Prieto C, Martinez-Marcos A (2014) Alpha-Synuclein in the olfactory system in Parkinson's disease: role of neural connections on spreading pathology. *Brain Struct Funct* 219(5):1513–1526
80. Ubeda-Banon I, Saiz-Sanchez D, de la Rosa-Prieto C, Mohedano-Moriano A, Fradejas N, Calvo S, Argandona-Palacios L, Garcia-Munozguren S, Martinez-Marcos A (2010b) Staging of alpha-synuclein in the olfactory bulb in a model of Parkinson's disease: cell types involved. *Mov Disord* 25(11):1701–1707
81. Ulusoy A, Rusconi R, Perez-Revuelta BI, Musgrove RE, Helwig M, Winzen-Reichert B, Di Monte DA (2013) Caudo-rostral brain spreading of alpha-synuclein through vagal connections. *EMBO Mol Med* 5(7):1119–1127
82. Volpicelli-Daley L, Brundin P (2018) Prion-like propagation of pathology in Parkinson disease. *Handb Clin Neurol* 153:321–335
83. Walker LC, Jucker M (2015) Neurodegenerative diseases: expanding the prion concept. *Annu Rev Neurosci* 38:87–103

Ready to submit your research? Choose BMC and benefit from:

- fast, convenient online submission
- thorough peer review by experienced researchers in your field
- rapid publication on acceptance
- support for research data, including large and complex data types
- gold Open Access which fosters wider collaboration and increased citations
- maximum visibility for your research: over 100M website views per year

At BMC, research is always in progress.

Learn more biomedcentral.com/submissions

